Comparison of Ichimura-Austern-Vincent and Glauber models for the deuteron-induced inclusive breakup reaction in light and medium-mass nuclei

Hao Liu,[1] Shinsuke Nakayama,[2,*] Jin Lei[1,†] and Zhongzhou Ren[1]

[1]*School of Physics Science and Engineering, Tongji University, Shanghai 200092, China*
[2]*Nuclear Data Center, Japan Atomic Energy Agency, Tokai-mura, Naka-gun, Ibaraki 319-1195, Japan*

This study focuses on the deuteron-induced inclusive breakup reaction and investigates the (d, pX) and (d, nX) channels for light and medium mass nuclei. To study the double differential cross section of nonelastic breakup, we employed the models of Ichimura, Austern, and Vincent (IAV) [Phys. Rev. C **32**, 431 (1985)] and the Glauber model with the quantum S matrix [Phys. Rev. C **80**, 014604 (2009)], and compared the results for various reaction systems. Our analysis indicates that the Glauber model combined with the quantum S matrix yields good agreement with the IAV model in predicting the spectra of the deuteron-induced inclusive breakup cross section. Moreover, both models accurately predict the experimental data of light and medium mass targets.

I. INTRODUCTION

Nuclear reactions can provide information about the structure of nuclei. Recent theoretical and experimental studies have focused on the breakup reaction, which is a critical process in reactions that involve weakly bound nuclei [1–11]. Among these reactions, deuteron-induced inclusive breakup reactions have been particularly important. These reactions are the processes in which a deuteron collides with a target nucleus and breaks up into a proton and neutron, allowing researchers to measure one fragment, either proton or neutron, without needing to detect the remaining system (shown in Fig. 1). They have been a variety of applications, including the synthesis of medical radioisotopes [12] and the utilization of deuteron accelerators as intensive neutron sources [13]. And also these reactions can provide valuable information about nucleosynthesis in stars, particularly in regards to the production of light elements such as Li, Be, and B [14]. Nonetheless, presenting an accurate description of inclusive reactions is a challenging task for basic nuclear research since several channels are involved. Such descriptions are critical for effectively testing the accuracy of reaction mechanism models and determining nuclear reaction data.

Recently, the (d, nX) reaction on light nuclei, including Li, Be, and C, is seen as a promising means of generating intense neutron beams in the facilities [15]. These neutron sources have been suggested for various applications, including scientific projects, such as the International Fusion Materials Irradiation Facility (IFMIF) [13], and also medical applications, such as boron neutron capture therapy (BNCT) [16]. Therefore, the design of accelerated neutron sources requires comprehensive and accurate nuclear data on deuteron-induced reactions across a wide range of nuclei, including Fe, Cr, Ni, which are materials used in the construction of accelerators, and targets. Nevertheless, there is a lack of experimental data on these reactions. Thus, to investigate inclusive breakup reactions, different reaction models have been employed, including the continuum-discretized coupled-channels (CDCC) method. Studies have indicated that the CDCC method is reliable in computing elastic breakup (EBU) which pertains to the fragmentation into fragments with their ground states [17,18]. A compound system can form from the combination of the deuteron and target followed by releasing neutrons or protons through pre-equilibrium and compound processes. These processes can be analyzed by the moving source (MS) model [19], the exciton and Hauser-Feshbach models, which were mentioned in Refs. [20–22]. This study concentrates on computing nonelastic breakup (NEB), popularly known as the stripping process. The process refers to breakup procedures that entail the incorporation of fragments or target excitation and the absorption of fragments into the target.

Recently, an integrated code system, DEURACS (DEUteron-induced Reaction Analysis Code System), has been developed to describe deuteron-induced reactions and has been successfully used in analyzing (d, nX) and (d, pX) reaction data [15,23–25]. DEURACS consists of various theoretical models that utilize several calculation methods to describe unique reaction mechanisms for deuteron-induced reactions. EBU is calculated using the CDCC method. In addition, the CCONE system has been utilized to derive the preequilibrium and compound nucleus processes. NEB, a combination of spectator neutron (or proton) and participant proton (or neutron), has been derived using the semiclassical Glauber model (GM), benefiting from the use of eikonal and adiabatic approximations. The cross sections of NEB were computed using the unitarity of the proton (or neutron) S matrix.

On the other hand, the fully quantum-mechanical model proposed by Ichimura, Austern, and Vincent (IAV) was

*Corresponding author: nakayama.shinsuke@jaea.go.jp
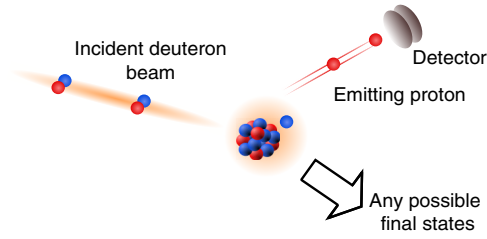†Corresponding author: jinl@tongji.edu.cn

FIG. 1. The deuteron-induced inclusive breakup reaction.

introduced in the 1980s to describe the inclusive breakup reaction. But unfortunately, this work did not receive widespread attention after a while. Until the last ten years, the IAV model was reintroduced and applied to a variety of unstable or stable nuclei [2–6,10,11,26,27]. Previous studies have proven the reliability of the IAV model in predicting the production of the deuteron-induced inclusive breakup reaction cross section [2–6,10,11,26].

The reliability of the GM has been questioned in a wider range of physical scenarios due to its semiclassical approximation. This study examines the reliability of GM by using the fully quantum mechanical IAV model.

In the present work, both the GM with the quantum S matrix, which is carried out in the DEURACS, and IAV model are employed to calculate the double differential cross section of NEB. To compare with the experimental data, the ^{58}Ni(d, pX) and ^{12}C(d, pX) at 56 MeV and 100 MeV are considered. In addition, the calculations of ^{58}Ni(d, nX) and ^{12}C(d, nX) at the same incident energies are carried out.

The paper is structured as follows. In Sec. II, we briefly review the IAV model and Glauber model. In Sec. III, the input parameters are listed here, and the numerical results of IAV are presented and compared to experimental data and the Glauber model. Finally, a summary and conclusion are given in Sec. IV.

II. METHOD

A. IAV model

We briefly cover the model of Ichimura, Austern, and Vincent in this part. In order to address the inclusive breakup reaction, the IAV model was initially developed in the 1980s [28]. The reaction under study is considered as

$$a(= b + x) + A \rightarrow b + B^*, \quad (1)$$

where a is the projectile composed of $b + x$, which collides with target A, leaving the resident system $B^*(= A + x)$ by emitting the fragment b. And the resident system B^* can be in any possible final state.

The double differential cross section of NEB can be written as [28,29]

$$\frac{d^2\sigma}{dE_b d\Omega_b}\bigg|_{\text{NEB}} = -\frac{2}{\hbar v_i} \rho_b(E_b) \langle \psi_x(\boldsymbol{k_b})|W_x|\psi_x(\boldsymbol{k_b})\rangle, \quad (2)$$

where $\rho_b(E_b) = \mu_b k_b/(8\pi^3\hbar^2)$ is the density of states with μ_b the reduced mass of $b + B$ and their relative wave number k_b, and v_i is the projectile-target relative velocity in the incident

channel. The wave function, denoted ψ_x, for the x channel can be obtained by solving the inhomogeneous differential equation:

$$(E_x - K_x - U_{xA})\psi_x(\boldsymbol{k_b}, \boldsymbol{r_x}) = \langle \boldsymbol{r_x}\chi_b^{(-)}(\boldsymbol{k_b})|V_{\text{post}}|\chi_a^{(+)}\phi_a\rangle, \quad (3)$$

where $E_x = E - E_b$, K_x represents the kinetic energy operator for the relative motion between fragment x and target A, U_{xA} indicates the participant-target optical potential, and $\chi_b^{(-)}$ is the scattering wave function with the incoming boundary condition describing the scattering of b in the final channel in relation to the $x + A$ subsystem. Furthermore, $V_{\text{post}} = V_{bx} + U_{bA} - U_b$ illustrates the post-form transition operator, where V_{bx} represents the potential binding two clusters b and x in the initial composite nucleus a, U_{bA} is the spectator-target interaction, U_b shows the optical potential between the spectator b, and the subsystem of $x + A$, $\chi_a^{(+)}$ represents the distorted wave describing the $a + A$ elastic scattering with the outgoing boundary condition, and ϕ_a indicates the initial ground state of the projectile a.

B. Glauber model

The following section briefly explains the Glauber model; a semiclassical model that uses eikonal and adiabatic approximations. The development of the GM in the 1950s [30] allowed for the analysis of reactions induced by high-energy particles. The GM states that the differential cross section of NEB in the center of mass of the p-n system can be expressed as

$$\frac{d\sigma_{\text{NEB}}}{d\boldsymbol{k_b}} = \frac{1}{(2\pi)^3} \int d\boldsymbol{b_x} \left\{ |1 - |S_x|^2| \times \left| \int d\boldsymbol{r} e^{-ik_b \cdot r} S_b \psi_a(\boldsymbol{r}) \right|^2 \right\}, \quad (4)$$

where $\boldsymbol{b_x}$ is the impact parameter of particle x, S_x, and S_b are the S matrices of participate x and spectator b with respect to the target A, $\boldsymbol{r}$ is the relative coordinate between fragment x and fragment b in projectile, $\boldsymbol{k_b}$ is the vector of proton wave number, and ψ_a is the wave function of the projectile's ground state. In Eq. (4), the proton is assumed as the spectator. NEB emitting neutron is calculated by replacing the roles of participate and spectator in Eq. (4) comparing to the emitting proton case.

The double differential cross sections in the laboratory system are obtained as

$$\frac{d^2\sigma}{dE_b d\Omega_b}\bigg|_{\text{NEB}} = \frac{m_b k_b^L}{\hbar^2} \frac{d\sigma_{\text{NEB}}}{d\boldsymbol{k_b}}, \quad (5)$$

where m_b and k_b^L are the mass and the wave number in the laboratory system of particle b, respectively.

The original GM expressed in Eq. (4) employs the the eikonal phase shifts. In the present study, we perform the calculations by replacing the S matrix used in the semiclassical framework with those acquired from the optical model calculation, so as to consider the quantum mechanical effects. This approach was previously introduced in Ref. [17] and has subsequently been adopted in DEURACS.

TABLE I. Input parameters used in the IAV calculation.

Proton and neutron potential	Koning-Deraloche [34]
Deuteron potential	An-Cai [31]
Deuteron binding potential	Woods-Saxon form
	$r_0 = 1.25$ fm, $a = 0.65$ fm

C. Calculation method for deuteron

From deuteron-induced reactions, inclusive proton emission double differential cross sections contain contributions from a variety of reaction processes, including direct processes like EBU, NEB, and statistical processes like pre-equilibrium and evaporation. The inclusive reaction double differential cross section can be divided into three components as a result of the various reaction processes:

$$\frac{d^2\sigma_{(d,pX)}}{dEd\Omega} = \frac{d^2\sigma_{(d,pX)}^{EBU}}{dEd\Omega} + \frac{d^2\sigma_{(d,pX)}^{NEB}}{dEd\Omega} + \frac{d^2\sigma_{(d,pX)}^{PE+CN}}{dEd\Omega}, \quad (6)$$

where $d^2\sigma_{(d,pX)}^{EBU}/dEd\Omega$, $d^2\sigma_{(d,pX)}^{NEB}/dEd\Omega$, $d^2\sigma_{(d,pX)}^{PE+CN}/dEd\Omega$ correspond to the double differential cross sections for EBU, NEB, and statistical decay which includes the pre-equilibrium emission and evaporation from the compound nucleus (here, we note these processes as PE + CN), respectively.

First, the CDCC can be used to directly calculate the EBU component. And the PE+CN component is calculated by CCONE [20], which applies the Hauser-Feshbach and exciton models to describe this processes.

We take the result of EBU and PE+CN from the Ref. [15] and focus on the comparison of NEB for these two models. To simply the calculation, the inherent spins are disregarded.

III. NUMERICAL RESULTS

A. Input parameters

The optical potential is main input in our calculations. The final predictions may be influenced by choices of the neutron and proton potentials as well as the deuteron potential. Several studies have already examined the significance of optical potentials in the effects of deuteron-induced reactions [31–33].

Thus, in the calculation of the NEB, we employ the same potentials as in Ref. [21], which are also applied in the GM calculations with the quantum S matrix. Table I presents the parameters and models of the utilized optical potentials. Global optical potentials of Koning and Delaroche (KD) [34] are employed for neutron and proton. The deuteron potential used is the global deuteron optical potentials of An and Cai [31]. We assume that deuteron binding potential is in the form of Woods-Saxon shape. And its radius and diffuseness parameters are given in Table I. The depth of it is adapted to the binding energy of deuteron. In present work, the spin-term potential is not considered during the calculation.

B. Calculation for (d, pX) reaction

We analyzed the (d, pX) reactions with ^{12}C and ^{58}Ni targets at incident energies of 56 MeV and 100 MeV. We focused our analysis on the double differential cross section at

outgoing proton angles of 9.5° and 10.0° in the laboratory frame, where NEB components dominate the direct processes. Herein, we present the $d^2\sigma/dEd\Omega$ results obtained from the models utilized and compare them with the experimental data [35,36].

Figure 2 illustrates the double differential cross section of ^{12}C(d, pX) at incident energies of 56 MeV and 100 MeV as a function of outgoing proton energies at fixed angles of 9.5° and 10° in laboratory frame. The left panels (a) and (c) show the inclusive cross sections of ^{12}C(d, pX). The experimental data were taken from Refs. [35,36]. The inclusive cross section calculations with the IAV and GM models with the quantum S matrix are depicted using solid and dashed lines, respectively. The results demonstrate good agreement with the experimental data. Panels (a) and (c) reveal two peaks: a narrow peak in the low emission-energy range that corresponds to the PE+CN processes and a broad peak at half of the incident energy contributed by NEB. The right panels (b) and (d) of Fig. 2 present the NEB results. Both IAV and GM with the quantum S matrix depict a bell-shaped energy distribution with peaks at half of the incident energy. Overall, the two models provide the same shape and magnitude and exhibit good agreement across the energy range. Nevertheless, differences are still present in the NEB double differential cross section at lower outgoing proton energies. However, the impact of these differences on the agreement level between experimental data and the inclusive cross section shown in panels (a) and (c) of Fig. 2 is insignificant.

Figure 3 shows the results of ^{58}Ni(d, pX) at the incident energy of 56 MeV and 100 MeV in the laboratory frame. Similarly, the experimental data were obtained from Refs. [35,36] and is represented by circles. The double differential cross sections of NEB as a function of emitted proton energy in the laboratory frame are presented as dashed (GM) and solid (IAV) lines in logarithmic scale in Figs. 3(b) and 3(d), respectively. Similarly to the ^{12}C(d, pX) reaction, differences are observed in the NEB double differential cross section of the ^{58}Ni(d, pX) reaction. However, as shown in Figs. 3(a) and 3(c), these differences do not significantly affect the agreement of the experiment with the inclusive cross section.

Furthermore, as illustrated in Figs. 2 and 3, the results obtained from the GM model using the quantum S matrix disagree with the IAV model when the outgoing proton energy is high. In the high-energy region, energy conservation dictates low neutron energies with respect to the target, rendering the semiclassical GM model unsuitable and resulting in differing NEB cross sections compared to IAV. The similar result can also be observed at lower outgoing proton energies.

However, these differences in the lower outgoing proton energies can be disregarded in actual applications. Since the PE+CN process constitutes the majority of the inclusive double differential cross section in the region with low emission energy, the differences between the two models have little impact on the inclusive cross section.

Figure 4 displays the double differential cross section for ^{56}Ni(d, pX) at 56 MeV as a function of the emitted proton angles in the laboratory frame for different emitted energies, calculated using the GM model with the quantum S matrix and the IAV model. The logarithmic scale plot shows the
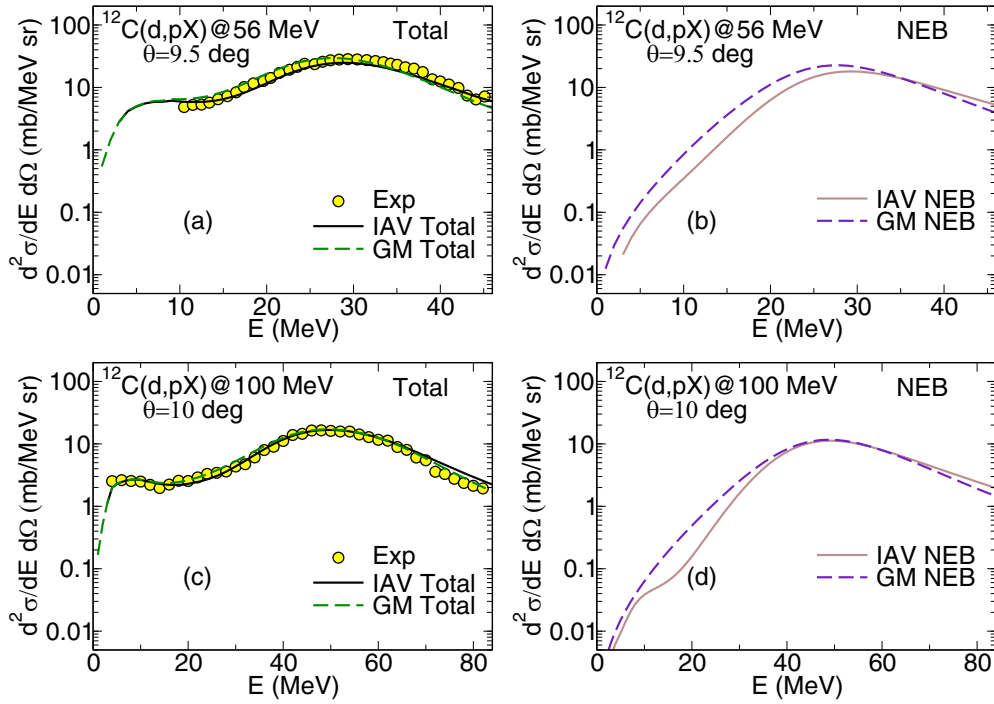
FIG. 2. Experimental and theoretical double differential cross section, as a function of emitted proton energy, for the protons emitted in the ^{12}C(d, pX) with angles of 9.5° and 10.0° in the laboratory frame, at incident energy of 56 MeV and 100 MeV. The inclusive double differential cross sections determined using the GM with the quantum S matrix (dashed line) and IAV model (solid line) are shown in the left panels [(a) and (c)]. And the experimental data are the circles which are from Refs. [35,36]. The contribution of the NEB calculated by the IAV (solid line) and GM with the quantum S matrix (dashed line), as illustrated in the right panels [(b) and (d)].
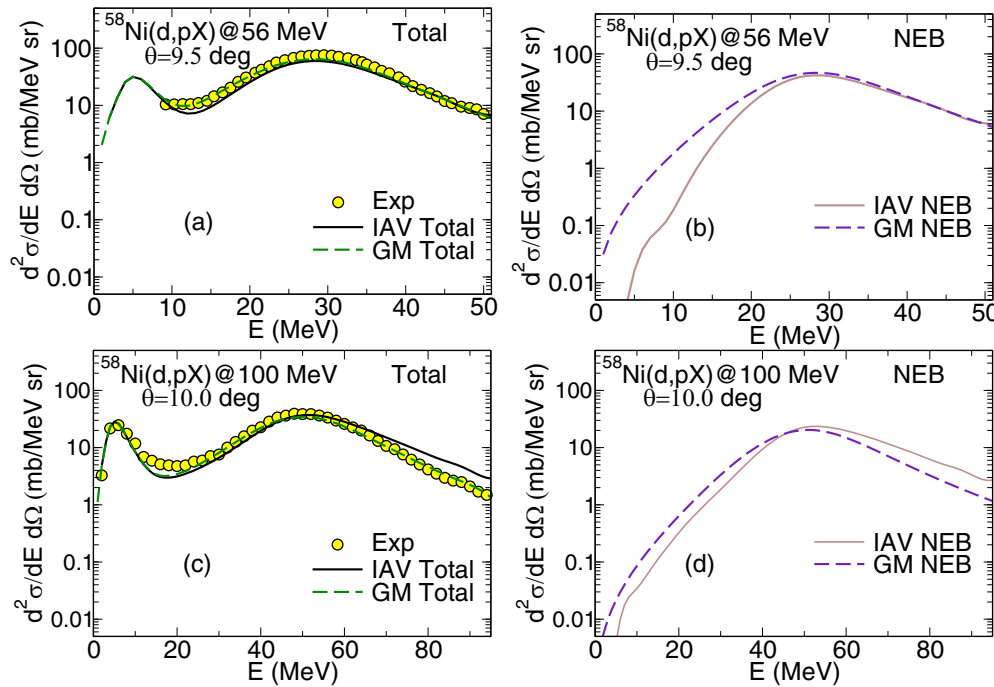

FIG. 3. Experimental and theoretical double differential cross section, as a function of emitted proton energy, for the protons emitted in the ^{58}Ni(d, pX) with angles of 9.5° and 10.0° in the laboratory frame, at incident energy of 56 MeV and 100 MeV. The inclusive double differential cross sections determined using the GM with the quantum S matrix (dashed line) and IAV model (solid line) are shown in the left panels [(a) and (c)]. And the experimental data are the circles which are from Refs. [35,36]. The contribution of the NEB calculated by the IAV (solid line) and GM with the quantum S matrix (dashed line), as illustrated in the right panels [(b) and (d)].
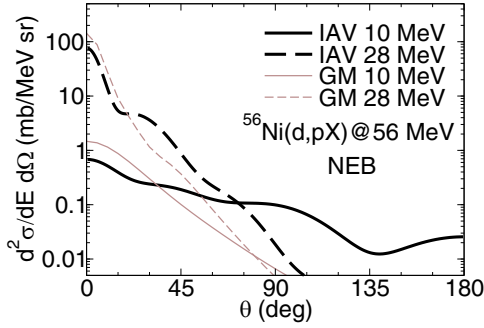
FIG. 4. Double differential cross section of NEB, as a function of emitted proton angles, in the laboratory frame, for the proton emitted in the ^{58}Ni(d, pX) at incident energy of 56 MeV, calculated by GM with the quantum S matrix (thinner lines) and IAV (thicker lines), respectively.

angular distributions of different outgoing proton energies, represented by thick lines corresponding to the IAV model and thinner lines relating to GM with the quantum S matrix. Solid and dashed lines represent outgoing proton energies of 10 MeV and 28 MeV, respectively.

First, both the IAV model and the GM model, with the quantum S matrix, have similar magnitudes, resulting in comparable integrated angular cross sections. Second, at higher emitted proton energies, the IAV model results concentrate more at the forward angles compared to the lower energies. On the other hand, the GM model with the quantum S matrix, produces a double differential cross section that concentrates more at the forward angles for both lower and higher energies. These results suggest that the GM model with the quantum S matrix, assumes a semiclassical picture by assuming a straight-line trajectory. Although the integrated angular cross sections of both models have similar magnitudes, their angular distributions are quite different. We conducted an analysis on the reaction (d, pX) using a lighter ^{12}C target at higher energies (100 MeV), resulting in a greater deviation from the Coulomb barrier than observed in the previous system, to gain additional insights. Our results, presented in Fig. 5, demonstrated that while the IAV model and GM, incorporating the
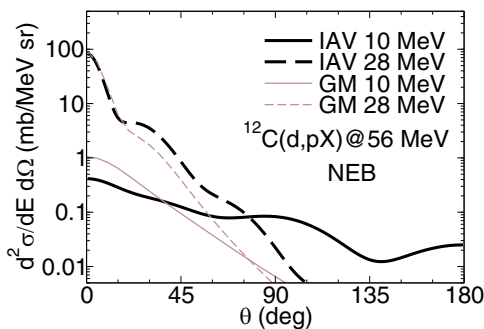

FIG. 5. Double differential cross section of NEB, as a function of emitted proton angles, in the laboratory frame, for the proton emitted in the ^{12}C(d, pX) at incident energy of 100 MeV, calculated by GM with the quantum S matrix (thinner lines) and IAV (thicker lines), respectively.

quantum S matrix, provided comparable outcomes for angular integrated cross sections, they produced significantly discordant results for angular distribution in double differential cross sections. These findings suggest that the angular distributions provided by the GM with the quantum S matrix are misaligned with those of the IAV model, even at higher energies. Nevertheless, previous studies [4,19] revealed that the PE+CN processes dominate in backward angles. Consequently, the differences between the GM with the quantum S matrix and IAV model are irrelevant to the inclusive consequences of (d, pX).

Generally, for the NEB process in (d, pX) reactions, the semiclassical GM model with the quantum S matrix provides cross section energy distributions that are in good agreement with the fully quantum IAV model. However, it should be noted that the GM with the quantum S matrix is itself a semiclassic model, and the quantum effects have not been fully considered.

C. Calculation for (d, nX) reaction

The double differential cross section of inclusive breakup (d, nX) can be represented similarly to the (d, pX) system, which is written as

$$\frac{d^2\sigma_{(d,nX)}}{dE\,d\Omega} = \frac{d^2\sigma_{(d,nX)}^{\text{EBU}}}{dE\,d\Omega} + \frac{d^2\sigma_{(d,nX)}^{\text{NEB}}}{dE\,d\Omega} + \frac{d^2\sigma_{(d,nX)}^{\text{PE+CN}}}{dE\,d\Omega}, \quad (7)$$

where $d^2\sigma_{(d,nX)}^{\text{EBU}}/dE\,d\Omega$, $d^2\sigma_{(d,nX)}^{\text{NEB}}/dE\,d\Omega$, $d^2\sigma_{(d,nX)}^{\text{PE+CN}}/dE\,d\Omega$ correspond to the double differential cross sections for EBU, NBU, and PE+CN, respectively.

Due to the scarcity of experimental data for (d, nX), we only compare the double differential cross sections of NEB computed by the IAV model and the GM with the quantum S matrix here. But it is important to note that the progress of the experiment has led to an increasing abundance of data in this area [1]. And the same potentials are adopted as (d, pX) reaction in the (d, nX) calculation. We also calculate the (d, nX) reactions for ^{12}C and ^{58}Ni, as the same incident energies and targets as these were calculated in the previous subsection, to make comparisons about (d, nX) and (d, pX) systems.

The double differential cross section of the NEB component for the (d, nX) reaction is displayed in Fig. 6 as a function of the outgoing neutron energy in the laboratory frame. The cross section is presented in logarithmic coordinates. Panels (a) and (c) on the left show the cross section with incident energy of 56 MeV when using ^{12}C and ^{56}Ni targets, respectively. Panels (b) and (d) on the right show the cross section with incident energy set at 100 MeV and using ^{12}C and ^{56}Ni targets, respectively.

The NEB cross section energy distribution computed by the IAV model and the GM with the quantum S matrix agree over the entire energy range, exhibiting a bell-shaped distribution peaking at half the incident energies, similar to the (d, pX) cases studied previously. The NEB cross section for (d, nX) is comparable to that of (d, pX), primarily due to Trojan horse effects, which suggest that the p and target Coulomb interaction have little impact on the NEB cross section. Differences between the two models become more apparent at higher energies (100 MeV) than at lower energies (50 MeV),
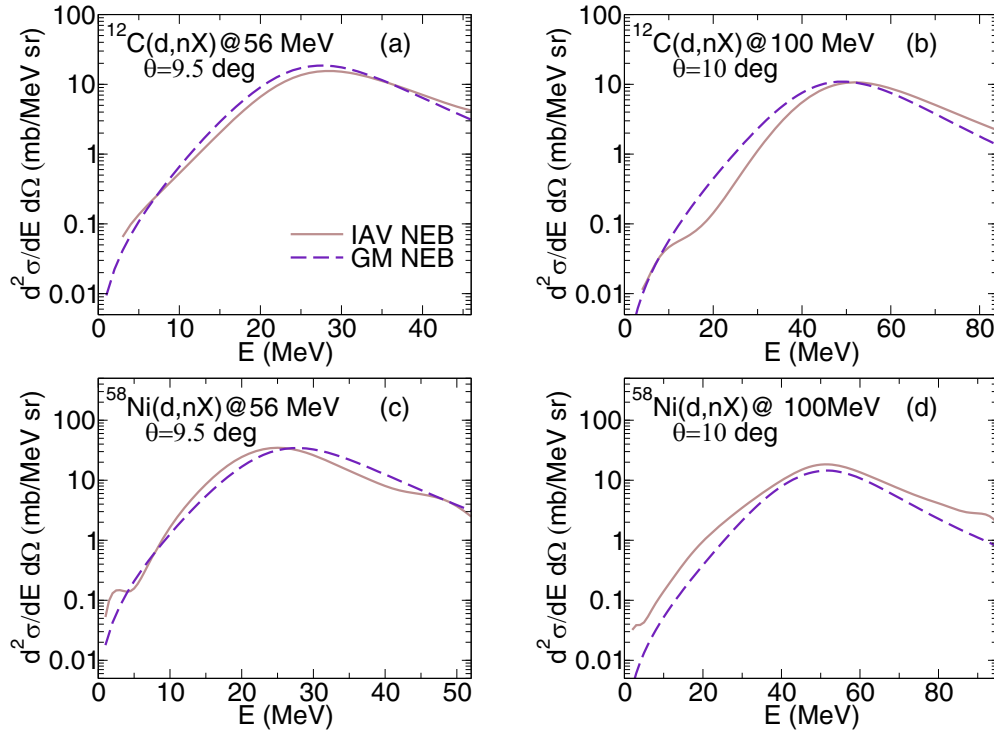
FIG. 6. The double differential cross section as a function of emitted neutron energy at angles of 9.5° and 10.0° in the laboratory frame from the ^{12}C(d, nX) and ^{58}Ni(d, nX) systems at incident energies of 56 MeV and 100 MeV. The solid line represents the result obtained using the IAV model. And the dashed lines represent the results obtained using the GM with the quantum S matrix.

partially due to the broader angular distribution computed by the IAV model, as previously observed in the (d, pX) case. This discrepancy will be explored further in the following.

In Figs. 7 and 8, we present the angular distribution of the double differential cross sections for the ^{12}C(d, nX) reaction at 100 MeV and ^{58}Ni(d, nX) reaction at 56 MeV, respectively, in logarithmic scale. The thinner and thicker lines indicate the GM with the quantum S matrix and the IAV model, respectively, with the dashed and solid lines depicting results at higher and lower outgoing neutron energies, respectively.

First of all, as can be seen in Fig. 7, the NEB cross section angular distribution computed by the IAV model for both lower (10 MeV) and higher (28 MeV) outgoing neutron energies has a significant contribution in both forward and backward angles, whereas the results obtained by GM with the quantum S matrix mainly concentrate at forward angles. Second, for the lighter target ^{12}C with higher incident energy of 100 MeV as one can see in Fig. 8, both the IAV model and GM with the quantum S matrix produce the cross section at the forward angles, in which the IAV model has a wider angular distribution compared to GM with the quantum S matrix. These observed trends align with those found in
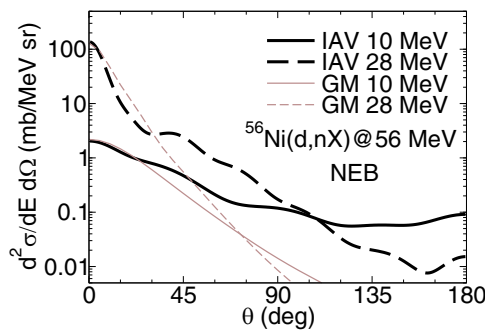

FIG. 7. Double differential cross section of NEB, as a function of emitted neutron angles, in the laboratory frame, for the neutron emitted in the ^{58}Ni(d, nX) at incident energy of 56 MeV, calculated by GM with the quantum S matrix (thinner lines) and the IAV model (thicker lines), respectively.
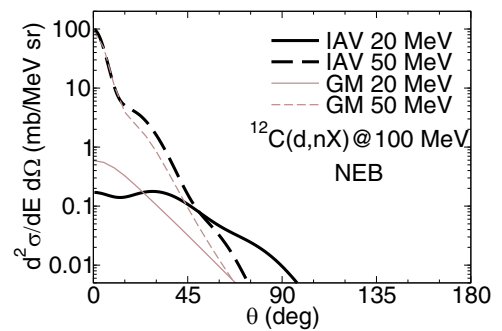

FIG. 8. Double differential cross section of NEB, as a function of emitted neutron angles, in the laboratory frame, for the neutron emitted in the ^{12}C(d, nX) at incident energy of 100 MeV, calculated by GM with the quantum S matrix (thinner lines) and the IAV model (thicker lines), respectively.

the (d, pX) case, justifying that the GM with the quantum S matrix is a semiclassical model that fails to accurately reproduce the angular distribution of the fully quantum IAV model.

IV. SUMMARY

In this article, the energy and angular distributions of both (d, pX) and (d, nX) reactions are investigated using the IAV model and GM with the quantum S matrix. The energy distribution results show similarities in shape and magnitude between the two models. However, differences are observed at lower and higher energies of outgoing spectators, primarily due to the limitations of the semiclassical model in the GM with the quantum S matrix.

The angular distributions for both reactions at light and medium mass targets with energies of 56 MeV and 100 MeV are also compared. The IAV model exhibits a wider range in angular distribution compared to the GM model with the quantum S matrix, indicating that the semiclassical model fails to reproduce the full quantum model.

In the inclusive measurement of (d, pX) and (d, nX), the contribution from backward angles mainly stems from PE+CN processes. This makes the differences between the IAV model and GM with the quantum S matrix less noticeable in the inclusive cross section.

The findings suggest that the IAV model has the potential to provide a more accurate explanation of the physical processes in inclusive breakup reactions than the GM model. However, further investigation and comparison with experimental data are necessary to determine the reliability and applicability of these models in various physical situations. Expanding the range of calculations to include additional inclusive breakup reactions will also help to better understand the differences between theoretical and experimental cross sections.

ACKNOWLEDGMENTS

[1] S. Araki, Y. Watanabe, M. Kitajima, H. Sadamatsu, K. Nakano, T. Kin, Y. Iwamoto, D. Satoh, M. Hagiwara, H. Yashima, and T. Shima, Nucl. Instrum. Methods Phys. Res. A **842**, 62 (2017).

[2] B. V. Carlson, R. Capote, and M. Sin, Few-Body Syst. **57**, 307 (2016).

[3] A. M. Moro and J. Lei, Few-Body Syst. **57**, 319 (2016).

[4] J. Lei and A. M. Moro, Phys. Rev. C **92**, 044616 (2015).

[5] J. Lei and A. M. Moro, Phys. Rev. C **92**, 061602(R) (2015).

[6] G. Potel, G. Perdikakis, B. V. Carlson, M. C. Atkinson, W. H. Dickhoff, J. E. Escher, M. S. Hussein, J. Lei, W. Li, A. O. Macchiavelli, A. M. Moro, F. M. Nunes, S. D. Pain, and J. Rotureau, Eur. Phys. J. A **53**, 178 (2017).

[7] M. Avrigeanu, E. Šimečková, U. Fischer, J. Mrázek, J. Novak, M. Štefánik, C. Costache, and V. Avrigeanu, Phys. Rev. C **101**, 024605 (2020).

[8] J. R. Wu, C. C. Chang, and H. D. Holmgren, Phys. Rev. C **19**, 370 (1979).

[9] A. Bonaccorso and D. M. Brink, Eur. Phys. J. A **57**, 171 (2021).

[10] L. J. Titus, F. M. Nunes, and G. Potel, Phys. Rev. C **93**, 014604 (2016).

[11] F. Torabi and B. V. Carlson, J. Phys. G: Nucl. Part. Phys. **50**, 045107 (2023).

[12] Y. Nagai, K. Hashimoto, Y. Hatsukawa, H. Saeki, S. Motoishi, N. Sato, M. Kawabata, H. Harada, T. Kin, K. Tsukada, T. K. Sato, F. Minato, O. Iwamoto, N. Iwamoto, Y. Seki, K. Yokoyama, T. Shiina, A. Ohta, N. Takeuchi, Y. Kawauchi *et al.*, J. Phys. Soc. Jpn. **82**, 064201 (2013).

[13] A. Moeslang, V. Heinzel, H. Matsui, and M. Sugimoto, Fusion Eng. Des. **81**, 863 (2006).

[14] J. E. Escher, J. T. Harke, F. S. Dietrich, N. D. Scielzo, I. J. Thompson, and W. Younes, Rev. Mod. Phys. **84**, 353 (2012).

[15] S. Nakayama, S. Araki, Y. Watanabe, O. Iwamoto, T. Ye, and K. Ogata, Energy Procedia **71**, 219 (2015).

[16] S. Agosteo, G. Curzio, F. d'Errico, R. Nath, and R. Tinti, Nucl. Instrum. Methods Phys. Res. A **476**, 106 (2002).

[17] T. Ye, S. Hashimoto, Y. Watanabe, K. Ogata, and M. Yahiro, Phys. Rev. C **84**, 054606 (2011).

[18] M. Yahiro, K. Ogata, T. Matsumoto, and K. Minomo, Prog. Theor. Exp. Phys. **2012**, 1A206 (2012).

[19] T. Ye, Y. Watanabe, and K. Ogata, Phys. Rev. C **80**, 014604 (2009).

[20] O. Iwamoto, N. Iwamoto, S. Kunieda, F. Minato, and K. Shibata, Nucl. Data Sheets **131**, 259 (2016).

[21] S. Nakayama, S. Araki, Y. Watanab, O. Iwamoto, T. Ye, and K. Ogata, Nucl. Data Sheets **118**, 305 (2014).

[22] T. Kawano, R. Capote, S. Hilaire, and P. Chau Huu-Tai, Phys. Rev. C **94**, 014612 (2016).

[23] S. Nakayama, H. Kouno, Y. Watanabe, O. Iwamoto, and K. Ogata, Phys. Rev. C **94**, 014618 (2016).

[24] S. Nakayama, N. Furutachi, O. Iwamoto, and Y. Watanabe, Phys. Rev. C **98**, 044606 (2018).

[25] S. Nakayama, O. Iwamoto, Y. Watanabe, and K. Ogata, J. Nucl. Sci. Technol. **58**, 805 (2021).

[26] G. Potel, F. M. Nunes, and I. J. Thompson, Phys. Rev. C **92**, 034611 (2015).

[27] J. Lei and A. M. Moro, Phys. Rev. C **95**, 044605 (2017).

[28] M. Ichimura, N. Austern, and C. M. Vincent, Phys. Rev. C **32**, 431 (1985).

[29] J. Lei and A. M. Moro, Phys. Rev. C **97**, 011601(R) (2018).

[30] R. J. Glauber, in *Lectures in Theoretical Physics*, edited by W. E. Brittin and L. G. Dunham (Interscience, New York, 1959), Vol. 1, pp. 315–414.

[31] H. An and C. Cai, Phys. Rev. C **73**, 054605 (2006).

[32] Y. Han, Y. Shi, and Q. Shen, Phys. Rev. C **74**, 044615 (2006).

[33] J. Bojowald, H. Machner, H. Nann, W. Oelert, M. Rogge, and P. Turek, Phys. Rev. C **38**, 1153 (1988).

[34] A. Koning and J. Delaroche, Nucl. Phys. A **713**, 231 (2003).

[35] D. Ridikas, W. Mittig, H. Savajols, P. Roussel-Chomaz, S. V. Förtsch, J. J. Lawrie, and G. F. Steyn, Phys. Rev. C **63**, 014610 (2000).

[36] N. Matsuoka, M. Kondo, A. Shimizu, T. Saito, S. Nagamachi, H. Sakaguchi, A. Goto, and F. Ohtani, Nucl. Phys. A **345**, 1 (1980).